Journal of Geography and Cartography 2025, 8(2), 11439.
https://doi.org/10.24294/jgc11439

Article

Detailed geophysical investigation consisted of electric and magnetic techniques carried out at Ancient Tritaea territory for location of subsurface archaeological finds

Panos Stephanopoulos[1,*], Stavros Papamarinopoulos[1], John Balatsas[2], Chistopher Kapopoulos[3], Lakaki Maria[4]

[1] Department of Geology, University of Patras, Laboratory of Geophysics, Rio, Patras, 26504 Achaea, Greece
[2] Geologist-Petrographer, Gounari5, Patras, 26221 Achaea, Greece
[3] Geologist-Civil Engineering, Gounari5, Patras, 26221 Achaea, Greece
[4] 6th Antiquity Service, Ypsilanti Alexandrou 197, Patras, 26225 Achaea, Greece
*** Corresponding author:** Panos Stephanopoulos, stefanop@upatras.gr

CITATION

Stephanopoulos P, Papamarinopoulos S, Balatsas J, et al. Detailed geophysical investigation consisted of electric and magnetic techniques carried out at Ancient Tritaea territory for location of subsurface archaeological finds. Journal of Geography and Cartography. 2025; 8(2): 11439. https://doi.org/10.24294/jgc11439

ARTICLE INFO

Received: 30 January 2025
Accepted: 13 March 2025
Available online: 7 May 2025

Abstract: A gradually detailed geophysical investigation took place on Ancient Marina territory. In that area was extended Ancient Tritaea, according to responsible Archaeological Services. The first approach had been attempted since 1988 by applied electric mapping based on a twin-probe array. Later, the survey extended to the peripheral zone under the relative request from the 6th Archaeological Antiquity. A new approach was implemented by combining three different geophysical techniques, like electrical mapping, total intensity, and vertical gradient. These were applied on discrete geophysical grids. Electric mapping tried to separate the area into low and high-interest subareas according to soil resistance allocation. That technique detected enough geometrical characteristics, which worked as the main lever for the application of two other geophysical techniques. The other two techniques would be to certify the existence of geometrical characteristics, which divorced them from geological findings. Magnetic methods were characterized as a rapid technique with greater sensitivity in relation to electric mapping. Also, vertical gradient focuses on the horizontal extension of buried remains. Processing of magnetic measurements (total and vertical) certified the results from electric mapping. Also, both of the techniques confirmed the existence of human activity results, which were presented as a cross-section of two perpendicular parts. The new survey results showed that the new findings related to results from the previous approach. Geophysical research in that area is continuing.

Keywords: geophysical investigation; electric mapping; total intensity; vertical gradient; Oasis Montaj

1. Introduction

A detailed geophysical investigation was applied gradually to Ancient Marina territory. Ancient Tritaea was one of the most well-known towns in ancient times. Geographically, it was placed about 31 km southwest from Patras, the capital city (**Figure 1**). The first approach of the geophysical survey had been applied since 1988 after the Antiquity request. During the first contact geophysics lab, the University of Patras accepted an investigation request from the Antiquity service (6th Antiquity Service). An experienced geophysical team applied geophysical survey by abutting specific geophysical instruments on the ground surface. As the main scope was the recording of fundamental properties of underground targets. Especially an investigation focused on the distribution of alteration of soil properties between underground targets and surrounding soil. Survey area divided by geophysical team in

common number of geophysical grids with acme equal to 20 m, by adopting Pythagoras Law in relation to measuring tapes. Each grid was surveyed with non-destructive [1–11] techniques such as electric mapping, total intensity, and vertical gradient. Corners and borders of grids were located on the ground by using non-magnetic materials like graduated rope with a red sign at one meter. Results from geophysical investigation discovered archaeological settlements, matters that demarcated them from geological structures. Clear geometrical characteristics were evidence of human activity, like a wall corner that was detected at 1.5 m depth [7]. After that matter, archaeological antiquity requested a new geophysical survey in the extended area of previously discovered archaeological remains. Another geophysical team accepted a new geophysical request and applied geophysical investigation towards existing remains during 1989–1990 in the second approach. As the main technique, electric mapping is applied by utilizing an electrometer such as Geoscan RM4 with four electrodes, based on the twin-probe technique [6–9]. Distribution of total intensity recorded by adopted two proton magnetometers type Elsec 820 [12–17]. Horizontal extension of magnetic structures obtained by using differential magnetometers such as Geoscan FM36 [3,6,9,18–20]. Measurements during the field procedure were stored inside the instrument data logger or alternatively on a geophysical grid hard copy. Later, measurements were transferred into laptop computers through RS232 special cable. By using Oasis Montaj software, the measured physical property was illustrated as a color map with a common color scale. Advanced geophysical interpretation applied on total and differential measurements.

Figure 1. Location of Ancient Marina (Ancient Tritaea) through the Google Earth application, with local coordinates. The red plate corresponded to the geophysical survey from 1988 to 1990.

2. Archaeological elements

Tritaea is mentioned as a city of the Achaean Dodecapolis. On the hill named Panagia, ruins were found that have been attributed to Ancient Tritaea after the discovery of an inscription in 1853, by resolution of the Achaean conference [21,22]. The site of the Archaic Tertiary was originally placed in different locations by various researchers, but the inscription led Ad. Wilhelm [23] in 1911 to concluded that the scattered ruins found on the said hill are identified with the Ancient Tritaea [21]. Based on studies [21–24], including younger scholars [25], confirmed and strengthened the above opinion that the specific location is identified with the Ancient Tritaea. Also, in the past, several inscribed tombstones from Hellenistic-Roman times have been collected from that hill [24,25]. Geographically, the city of Ancient Tritaea extends to the southernmost part of mountainous and inland Achaia. To the west it is bordered by Elida, Dimi, and Skollis Mountain. To the east it is defined by Erymanthos Mountain, while to the north it is surrounded by a growing series of contiguous hills. The development of the hills separates it from the Phares, which extend to the north. The same geomorphology separates it to the northeast from the area of ancient Leontium, while to the southeast from Lasonia. The hill of Panagia is bordered by two natural river branches of the Pinios river. The tributaries originate from Erymanthos Mountain, while towards the south side they join. Near the borders of Ancient Tritaea with Elis, the existence of a fortress can be found, which had the purpose of guarding the borders. Kelvidas from Kymi of the Opians (according to Pausanias) is considered the original inhabitant of this city, while other researchers support Melanippos, son of Ares and Tritia, daughter of Triton and the virgin Athena.

3. Geological regime

In Ancient Marina territory, appearances of sandstone flysch with conglomerate lenses consisting of pebbles of the Pindus series as well as mudstones with pebbles are shown in **Figure 2**. Benches with a thickness ranging between 2 and 15 m are found in **Figure 2**. That structure is characterized by a total thickness of approximately 1000 m (**Figure 2**). Blue siltstones with sandstones are present in that area with approximately a thickness of 1290 m. In some places, lateral embankments were illustrated in **Figure 2**, created by alluvium and short-distance flow. Also, there were blue siltstones with conglomerates and sandstones (**Figure 2**), which were characterized by a thickness of approximately 1290 m [26].

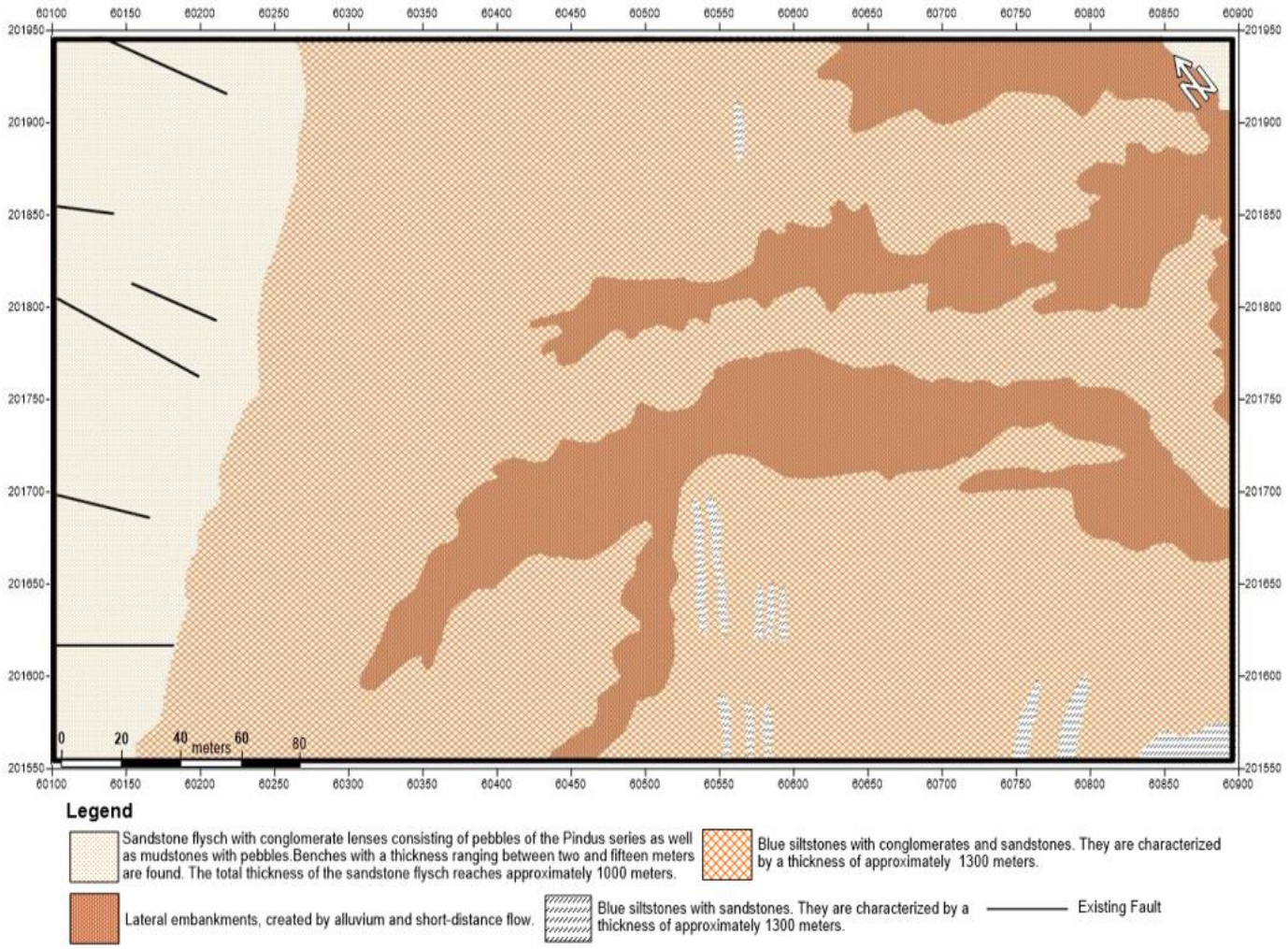

Figure 2. Geological map of Ancient Marina with local coordinates.

4. Methodology

On Tritaea territory (Saint Marina), detailed geophysical prospection was applied for the detection of underground settlements and remains.

- Area of interest divided into an able number of geophysical grids [8,9,13,27,28] with an acme of 20 m according to territory dimensions (**Figure 3**). On each grid, an electric and magnetic technique was applied with a non-destructive procedure.
- Discreet data point stations are located on sequence parallel profiles with intervals at one meter. The survey procedure began from the SW corner of each grid, while stations were distant 1 meter away along the South-North axis (**Figure 4**).
- Electric and magnetic instruments are checked in case of recording abnormal measurements.
- Orientation of geophysical grids occurred by using non-magnetic material, such as wooden sticks, and calibrated ropes [29,30].
- Area of interest was checked for the existence of magnetic garbage. Also, the ground surface was cleared of any existing plants and greens.

- Total intensity measurements were corrected for daily geomagnetic drift [9,12–15,31]. Also, base station measurements were graphically examined for the existence of bad datum points.
- Proton and differential magnetometers were adjusted on quiet magnetic points [32]. About the geomagnetic drift elimination, the internal clock of two proton magnetometers was synchronized.
- Data from the proton and fluxgate magnetometer was transferred to a PC through an RS232 cable, in relation to specific software [32].
- Interpretation of measurements accomplished by using mathematical algorithms of Oasis Montaj software [6,8,9,12,19,33–35].

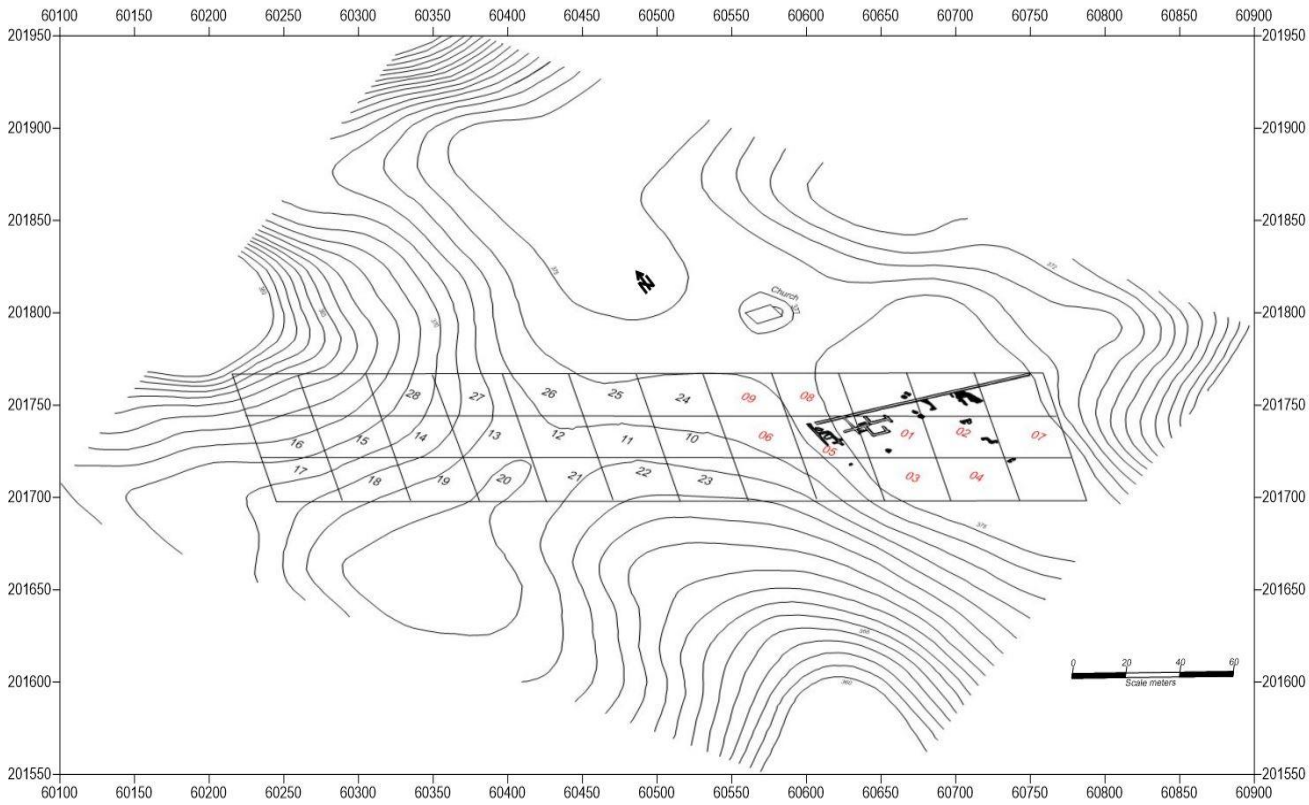

Figure 3. Classification of geophysical grids on the topographical map of Ancient Tritaea territory with local coordinates. (Red numbers corresponded in the initial investigation).

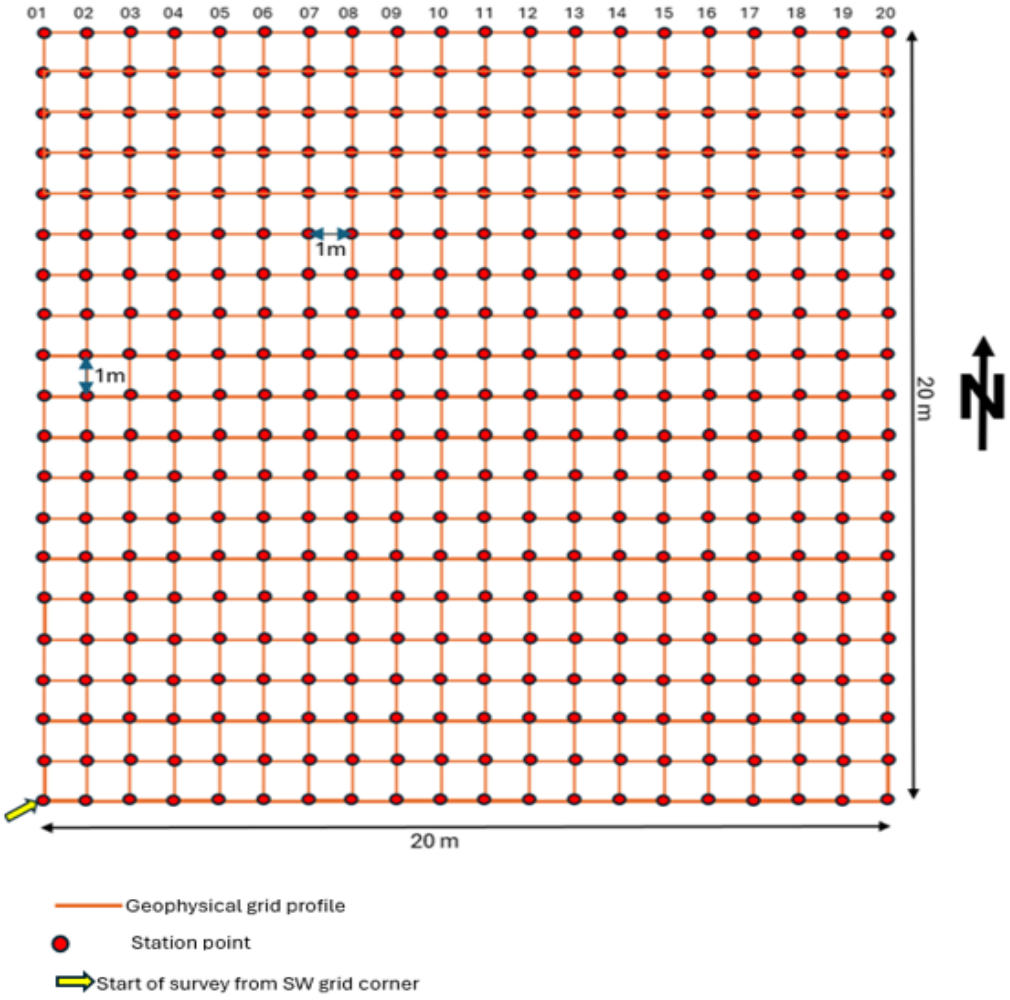

Figure 4. Schematical appearance of geophysical grid with parallel profiles, data stations and point of survey starting.

5. Instruments checking and adjustment

Checking and adjustment of geophysical instruments was one of the most critical points before the origination of the main survey procedure. Both electrometer and magnetic units were checked on purpose for abruption of measured properties pollution due to an external factor.

5.1. Checking of electrical technique

Electric mapping would be the fundamental technique that could easily divorce the territory in low and high-interest subareas. That procedure was based on the existence of one electrometer with special cables and steel electrodes. Arrangement of involved electrodes based on the twin-probe technique (**Figure 5**) [6,7,8,9,29]. According to that technique, there were two pairs of electrodes. Each of them consisted of one current and potential electrode. Each electrode pair was distant at 0.75 m. One pair was acting as a base and the second as mobile. The base station was set at a distance at least fifteen times the internal pair distance. The mobile pair was moving inside the geophysical grid profile, recording individual data points with an interval equal to one meter. For checking purposes, the role of mobile and stable pairs was gradually substituted. During electrode substitution, recordings of soil resistance are

obtained (**Figure 6**). The difference between those measurements should not be greater than one ohm. In that case, recording values were accepted and characterized as unpolluted records. In case of polluted values, the substitution procedure was continued until the recording of healthy measurements.

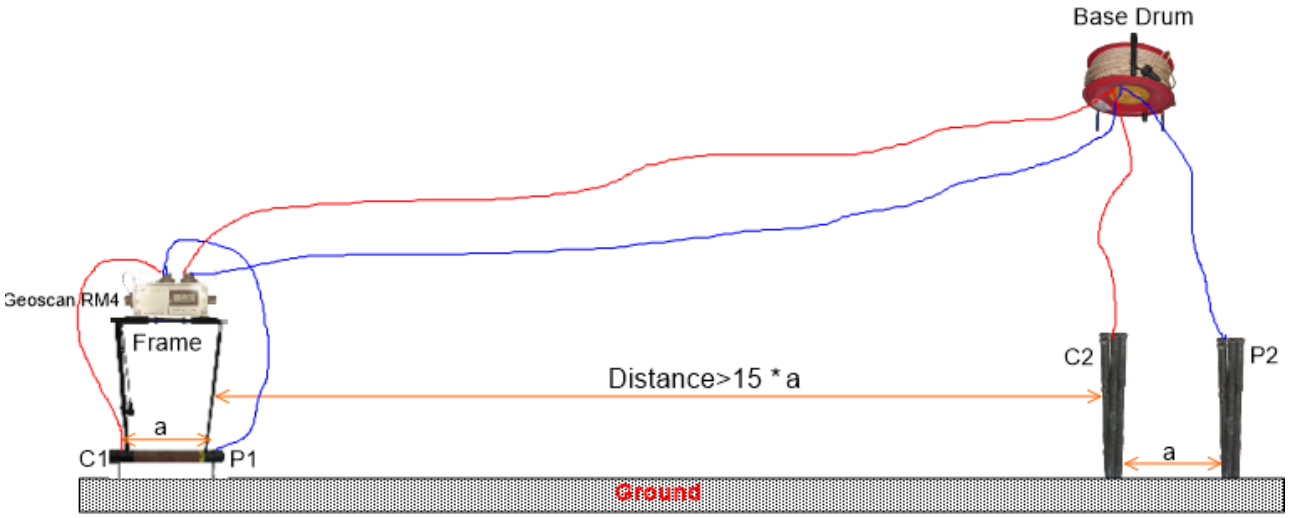

Electrometer Geoscan RM4
Frame : Mobile electrodes
C1: Current Electrode 1
P1: Potential Electrode 1
a: internal pair distance
Base drum: Extension cable for base electrodes
C2: Current electrode 2
P2: Potential Electrode 2

Figure 5. Electric mapping technique based on twin-probe arrangement.

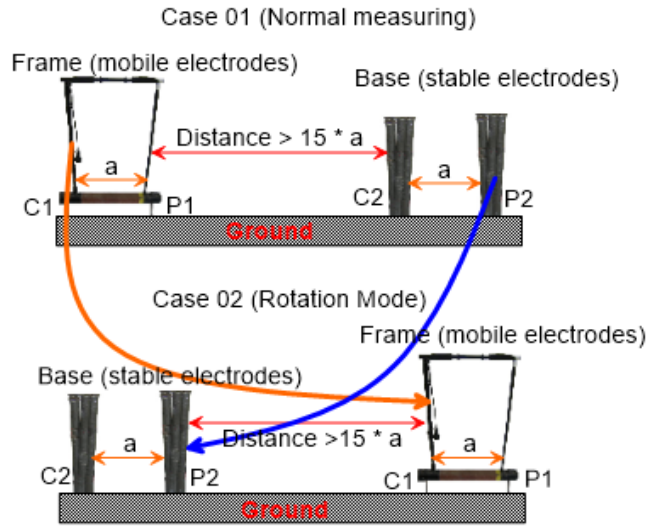

a : Internal Pair Distance
C1: Current Electrode 1
P1: Potential Electrode 1
C2: Current Electrode 2
P2: Potential Electrode 2
Case01: Initial measuring mode of twin-probe arrangement
Case02: Rotational mode between mobile (red arrow) and stable elcetrodes (blue arrow) for checking purposes

Figure 6. Gradually substitute mobile and stable electrodes for checking purposes.

5.2. Checking magnetic technique

Magnetic units were checked for the abruption of possible polluted values. The candidate area was examined for the existence of magnetic garbage, including iron, iron-fence, and antenna (mobile telephone, radio, TV) [32]. Also, existing greens were removed from the ground surface. Proton magnetometers were adjusted according to survey parameters by typing the value of geomagnetic intensity. In addition, the internal clock was synchronized in both instruments. That parameter was recorded during the field procedure for the correction of daily geomagnetic drift. One magnetometer was acting as a base and recording geomagnetic intensity values with intervals of ten seconds. The magnetometer sensor, which acted as a base, should be placed on a quiet magnetic point without any external influences. For collateral to that, independent values were recorded by rotation of magnetic sensors by an angle of 90° (**Figure 7**) [6,32]. Quite magnetically, that point was secured if the difference of four sequence recorded values was equal to one nT. In case of a recorded greater difference, the magnetic sensor was moved to another point, and the previous procedure was restarted.

On the same quiet magnetically point differential magnetometer was adjusted too. Before the vertical gradient survey procedure, it should be ensured that the gradiometer could not be polluted from an external factor in any direction. According to that vertical gradient, values were checked by rotating the differential magnetometer in five different directions (air, N, S, E, W) (**Figure 8**) [32]. During that procedure, the difference of recorded measurements should be equal to one nT/m. The next step was the adjustment of a gradiometer microcomputer with grid dimensions.

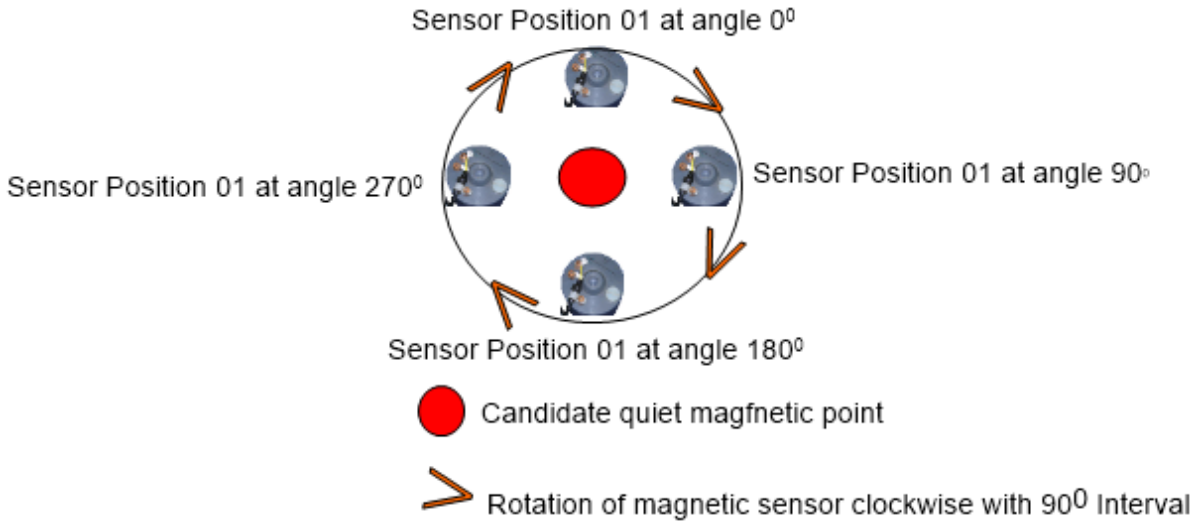

Figure 7. Quiet magnetic point examination.

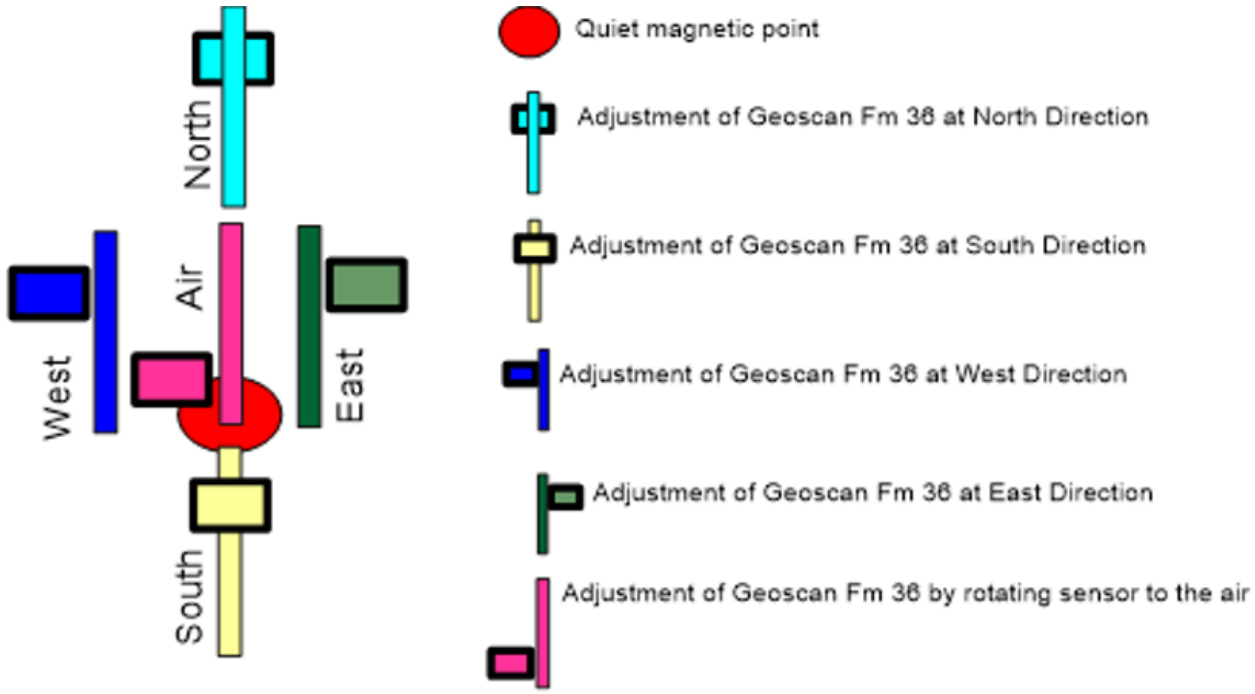

Figure 8. Adjustment of fluxgate unit on quiet magnetic point.

6. Electric and magnetic applications

A geophysical survey on Saint Marina territory was conducted gradually. At the beginning of the investigation, the area should be divided into subareas characterized as low and high interests. That role was assigned to electric mapping, a technique from the family of induced electric fields into the ground. Certification of underground settlements had been assigned to magnetic prospecting. Geophysical grids with red color corresponded in the initial geophysical investigation. Results from that survey are illustrated in **Figure 3**. Geophysical grids with black numbers referred to the extended survey that is mentioned in that manuscript.

6.1. Electric prospecting

Electric mapping was adopted as the main technique for detecting underground archaeological remains along horizontal layers. It was one of the most often used geophysical applications. Characterized with excellent results, while existing geometrical characteristics were recorded with huge clarity. That technique consisted of a combination of an electrometer, special cables, and steel electrodes (**Figure 9**). As the main electrometer, we utilized Geoscan Rm4 (**Figure 9**), which had the ability of soil resistance distribution according to Ohm's Law. Electric mapping is performed by utilizing a twin-probe arrangement, a technique independent from topographical allocations [6,9,32]. According to the twin-probe technique in **Figure 5**, electrodes were separated into two pairs, consisting of one current and potential electrode. The pairs' distance theoretically was equal to infinity. In practice, mobile and stable pairs were divorced at least fifteen times the fundamental distance (internal distance 0.75 m). Detection of underground targets occurred until a depth equal to three times the internal pair distance.

The position of stable electrodes was common for most geophysical grids. The base location had been arranged along intervertical grid lines [6,9,32]. During the field procedure, soil resistance distribution was recorded with the same location of base electrodes. Unfortunately, in some cases there was an imperative need for base electrode location removal. Most often justification was the problem with cable length between mobile and base electrodes. In that case, the new position of the base station should be examined for measurement pollution after the removal [32]. In that case, the last profile of the geophysical grid was repeated after the base electrodes were removed. The last profile of the geophysical grid was remeasured with the new location of the stable pair (**Figure 10**). Average values of the profile before (A1) and after pair removal (A2) were calculated. In case A1 was less than A2, the difference A2-A1 was added to A1 measurements or alternatively subtracted from A2 values (**Figure 10**). In case A1 was equal to A2, then correction of measured values was not a necessity. In cases where A1 was increased in relation to A2, the difference A1-A2 was added to A2 measurements or subtracted from A1 values, as shown in **Figure 10**. Values during the field procedure were stored on a hard copy of the geophysical grid or alternatively inside the memory of the data logger.

Figure 9. Electric mapping instruments consisted of an electrometer, special cable, mobile electrodes (frame), and steel electrodes.

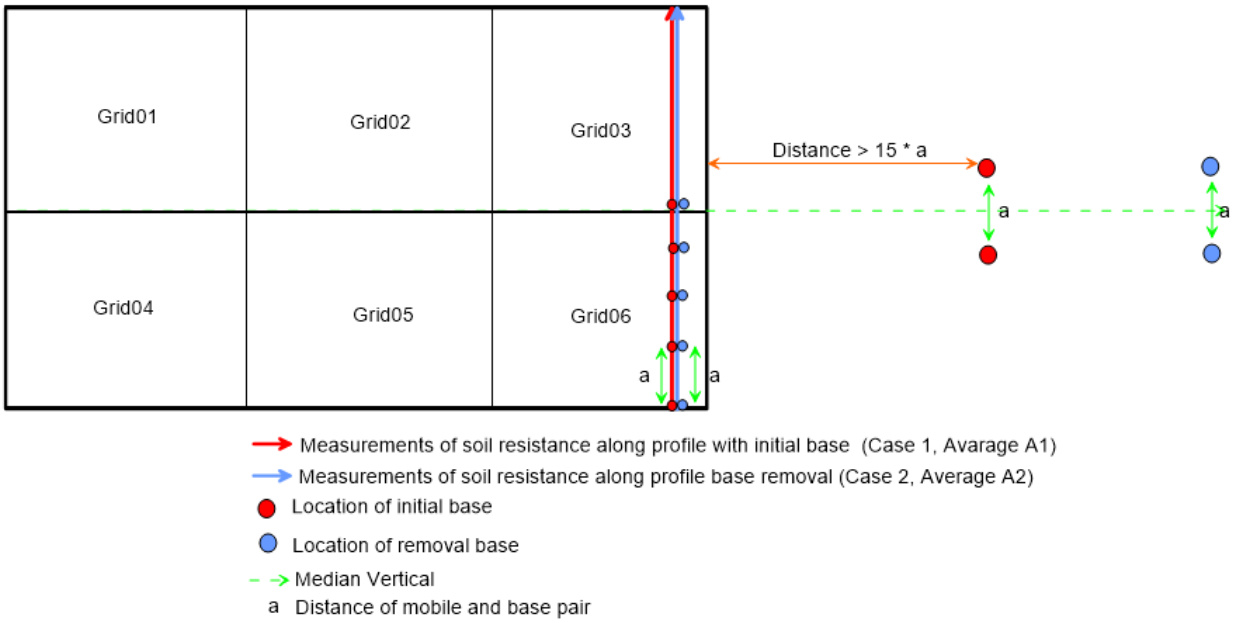

Figure 10. Application of twin-probe arrangement with mandatory movement of stable electrodes.

6.2. Magnetic prospecting

Geomagnetic techniques [2,3,9,12–17,33–36] referred to a very rapid prospection, focusing on the detection of underground magnetized bodies. The survey occurred by adopting two different kinds of magnetic instruments. Firstly, by utilizing the proton magnetometer type Elsec 820 (**Figure 11**), the distribution of geomagnetic intensity was recorded on discreet stations with an interval equal to one meter. Penetration depth was related to three to five times the magnetic sensor height above the ground surface (0.30 m). During prospection, adopted two of the same proton magnetometers. One of them was moving inside the geophysical grid in parallel profiles along the south-north axis with one-meter intervals. The second instrument was located on a magnetic quiet point and recorded daily geomagnetic drift every ten seconds. At every measure, the magnetic sensor was oriented parallel to geomagnetic north. Secondly, recording vertical gradients is applied by using a differential magnetometer. As a gradiometer [3,5,9,10,16] Geoscan FM36 is adopted in **Figure 12**. Before the main survey procedure, the fluxgate magnetometer was adjusted to a quiet magnetic point, as was mentioned in the previous adjustment paragraph. Discreet stations and profiles were lying along the South-North axis with intervals equal to one meter, while the sensor was located 0.5 m above the ground surface. Start points of measurements on each geophysical grid were set at the southwest corner (**Figure 4**).

Geophysical grids and corresponding profiles were signed by non-magnetic [6,9,32] material, like graduated ropes and wooden sticks. Each corner of the grid was given by inserting into the ground a wooden, red-colored stick. Directions of separated profiles were shown by using calibrated ropes [6,9,29,30] with a red sign every one meter. Two ropes were lying along the south and north borders of the grid, while the third rope was located perpendicular to the two previous ones.

Soil resistance distribution, total intensity, and vertical gradient measurements were reduced to a main level by applied common average value through statistical analysis [9].

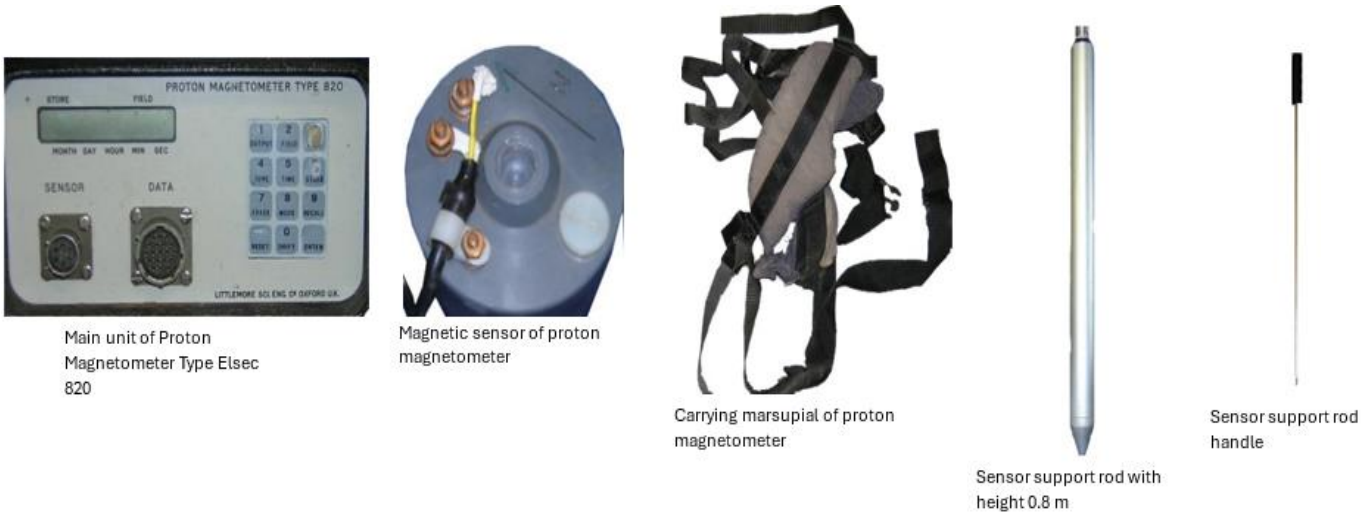

Figure 11. Total intensity prospecting conducted by proton magnetometer type Elsec 820.

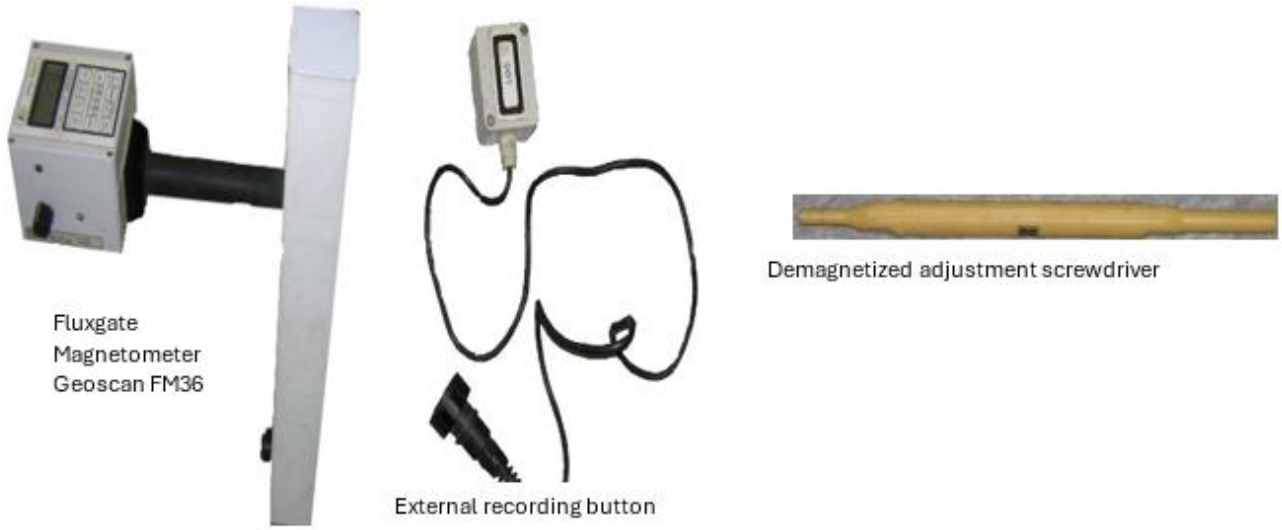

Figure 12. Fluxgate instrument with external recorded button and demagnetized screwdriver.

7. Interpretation of electric and magnetic measurements

Accomplishing the field procedure, where discrete points of physical property were recorded, now it was time for the level presentation of physical property. That procedure became a reality by processing recorded measurements from different instruments through dedicated geophysical software known as Oasis Montaj [6,8,9,12,19,33–35].

7.1. Main Interpretation of electric and magnetic measurements

During the field procedure, values were deposited inside the memory logger, or alternatives were typed on a hard copy of the grid schedule, with efforts made with

numbered rows and columns. In the case of data loggers, values were transferred to a PC through specific software in relation to the RS232 cable. In the case of the hard copy grid, the values were then transferred into the Surfer [6] worksheet in the same direction as they were recorded. A hard copy of the geophysical grid was used as a second solution in the case of the data logger multifunction, but also as a backup of measurements.

Values of field procedure corresponding to independent stations that were laid on the known location of the *x* and *y* axis (**Figure 3**). Drift geomagnetic correction was already applied on total intensity values. Base station values were examined for polluted measurements through graphical examination [6,9,32]. In the case of polluted values, these were rejected or substituted by statistical analysis [9]. Elimination of drift correction occurred by subtracting base values from mobile values relative to recorded time [9,32]. Through specific software or surfer subroutine values, dimensioned with known levels or geographical coordinates, a file of x, y, z mode is obtained. Accomplishment of dimensions and measurements was fed inside the Oasis Montaj worksheet for further processing. Geophysical grids from three different techniques were combined by calculating a common average value through statistical analysis. The first processing step was performed as an interpolation procedure [37]. By implementing the minimum curvature algorithm [37], discrete stations were combined by calculating new internal values using an interval step equal to 1/4 of the field procedure stations distance. For the presentation of physical property, a common color scale was developed with a corresponding common color zone and scale. The fluxgate magnetometer wasn't affected by daily magnetic drift. Values from both magnetometers were dimensioned according to level/geographical coordinates. Measurements were stored inside XYZ format files readable from Oasis Montaj processing software. On developed color maps, the distribution of physical properties such as soil resistance, total intensity, and vertical gradient was presented. For enhancing detailed findings, values were processed by mathematical equations based on shaded relief [9,37]. According to that, values were illuminated by a secondary light source. Some parts of the maps were brightly lit while others were covered by shadows. This kind of procedure had as a result the detailed findings promotion relative to the initial allocation of physical property. On electric mapping values, apply an analytic signal mathematical algorithm based on the Fast Fourier Transform [9,37].

7.2. Advanced processing of magnetic values

Advanced processing was performed on magnetic measurements. For the elimination of existing noise, we implemented a mathematical equation based on upward [6,9,32,35] and downward [6,9,14] continuation. The first filter (upward) agrees to eliminate noise while trying to remove existing noise from near-surface sources. The implementation of that filter had as a result the expansion of geophysical anomalies. The second filter (downward) agrees to transfer existing geophysical anomalies towards magnetic sources. Upward and downward continuation applied only on total intensity values for upward and downward processing at one meter included a smooth low-pass filter. As the next step, calculated the parameters of the magnetic field, such as inclination and declination, which were fundamental

parameters for reduction to the north magnetic pole and equator [37]. By utilizing special subroutines of Oasis Montaj software, a calculated illustration of values is present in the north magnetic pole [9,34] or magnetic equator [9,14,36,38]. These two filters had as a result the appearance of more detailed geophysical anomalies in relation to the initial geophysical maps. Reduction to the north magnetic pole could locate the geophysical anomalies over their sources [37]. While reduction to the magnetic equator is used to center the geophysical anomalies over their sources [37]. By applying a combination of downward continuation, reduction to the north pole, and relative mathematical equations, a distribution of apparent susceptibility [2,3,9,12,20,31,33,36,39] was obtained. That parameter expressed the height of possible magnetized bodies could be present at specific depths. Three-dimensional filter applied on magnetic measurements (total and gradient) for the detection of the source that had produced the magnetic geophysical anomaly. That mathematical equation was the 3D Euler deconvolution [6,9,19,32,34]. During implementation, the algorithm combines the magnetic elements of the source with it, calculating derivatives and yielding solutions through a theoretical window with known dimensions [6,9,32,38]. Each solution corresponded to a different index known as a structural index. The structural index corresponded to a solution that referred to the distance of a solution from the center of the theoretical window during Euler implementation. Different values related to different shapes of mathematical models (**Table 1**).

Table 1. Values of the structural index during Euler deconvolution and the corresponding mathematical model.

Structural Index Values	
Value	**Magnetic Field**
0	Contact/Step
1	Sill/Dyke
2	Cylinder/Pipe
3	Sphere/Barrel/Ordnance

8. Results obtained from geophysical prospecting

This paragraph is devoted to obtaining results from the application of geophysical techniques.

8.1. Results from electric prospecting

The result of electric mapping is reported in **Figure 13**. The twin-probe arrangement recorded soil distribution along a horizontal layer at a depth of 3 times [6,7,8,9,29,32] the internal pair electrodes distance (0.75 m). The initial presentation of that physical parameter detects the existence of targets with high resistance, which was referred to by the red color. These findings were characterized by well-defined geometrical characteristics. The implementation of the shaded relief filter certified the existence of geometrical characteristics. By processing soil resistance measurements through the Fast Fourier Transform filter, geometrical characteristics were defined with greater clarity. The distribution of soil resistance varies between 28 and 67 ohms.

Detected underground targets located at a depth approximately between 1.5 and 2.25 m.

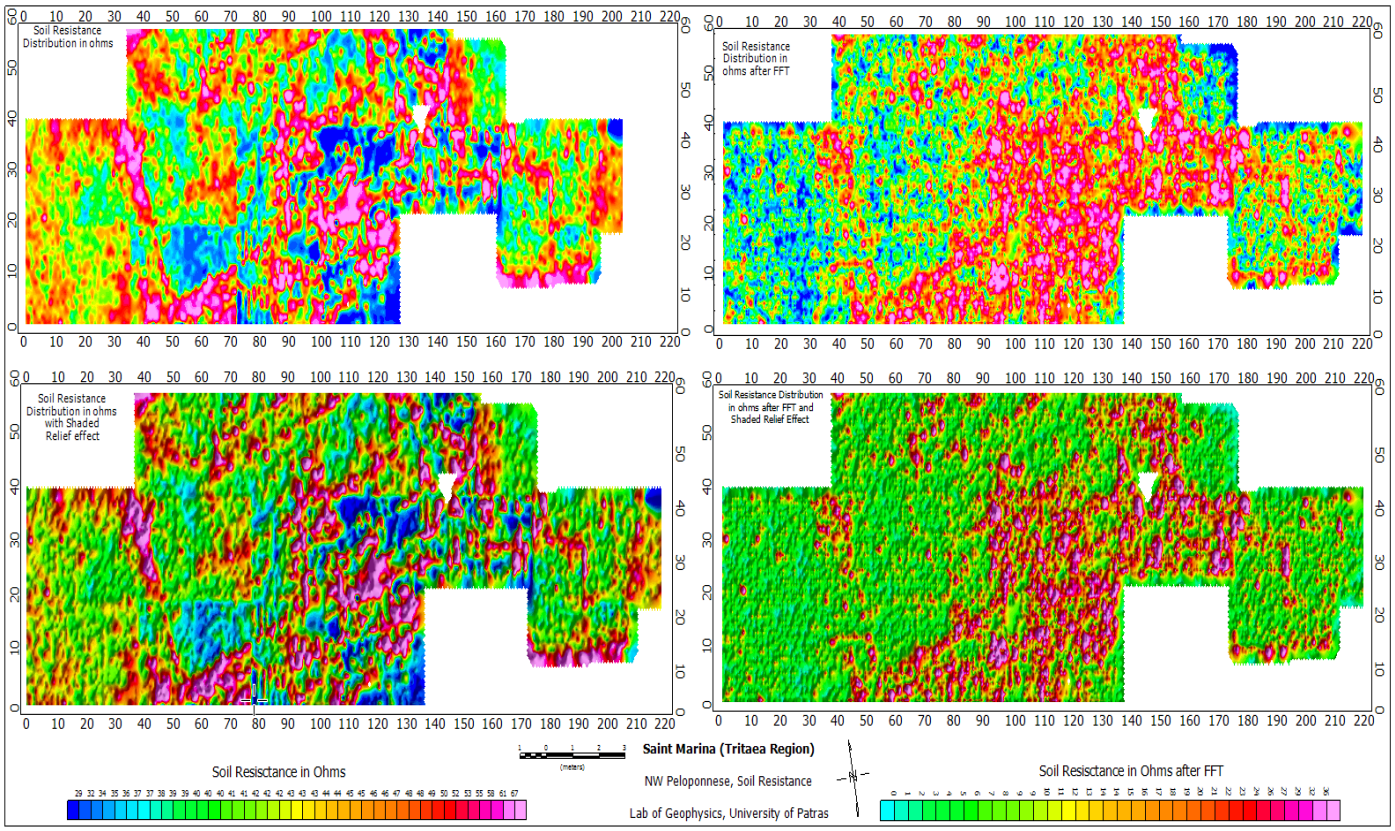

Figure 13. Distribution of soil resistance on Ancient Tritaea territory through twin-probe array, at 2.25 m depth.

8.2. Results from magnetic prospecting

Magnetic survey [2,3,9,12–17] was first applied by utilizing a proton magnetometer, which records the distribution of total intensity in nT (**Figure 14**). The magnetic sensor was anchored at 0.3 m above the ground surface and oriented along the geomagnetic north direction, while profiles and stations were distant at one meter. Penetration depth according to total sensor height was equal to 3 to 5 times the sensor height above the ground surface. That technique easily detected and clarified underground magnetized bodies, which were extended all over the magnetic map. Total intensity seemed to be varied between 45,870 and 45,906 nT. The initial presentation of total intensity points out clear geometrical characteristics, which seemed to be part of a huge corner. The implementation of the shaded relief filter certified the existence of geometrical characteristics, a matter that it confirmed as human activity and not a result of geological structure (**Figure 14**). Reduction to the north magnetic dipole verified the existence of magnetized bodies, which were classified as members of a huge geometrical structure, a result of human activity (**Figure 14**). Reduction to the magnetic equator illustrated partially the existence of magnetic bodies, with partial growth of geometrical characteristics. Now, the existing structure as a corner schedule was illustrated with low clarity (**Figure 14**). By further processing, we calculated the z gradient distribution (the fluxgate magnetometer was busy in another geophysical investigation that period) from total intensity

measurements (**Figure 15**) [3,5,6,9,17,37,40–43]. That mathematical filter breaks the existing targets into smaller parts. Now researchers can easily observe the existence of magnetic structures as part of two cross parts as a wall corner while showing another geometrical structure with smaller dilations at the southwest area of the z gradient map (**Figure 15**). Application of shaded relief certified the existence of two geometrical characteristics (**Figure 15**). Reduction to magnetic north and equator did not report geomagnetic anomalies with high distinct clarity (**Figure 15**). In some parts of the z gradient map, it just confirmed the existence of magnetic anomalies. Allocation of the z gradient seemed to be varied between −34 and 35 nT/m.

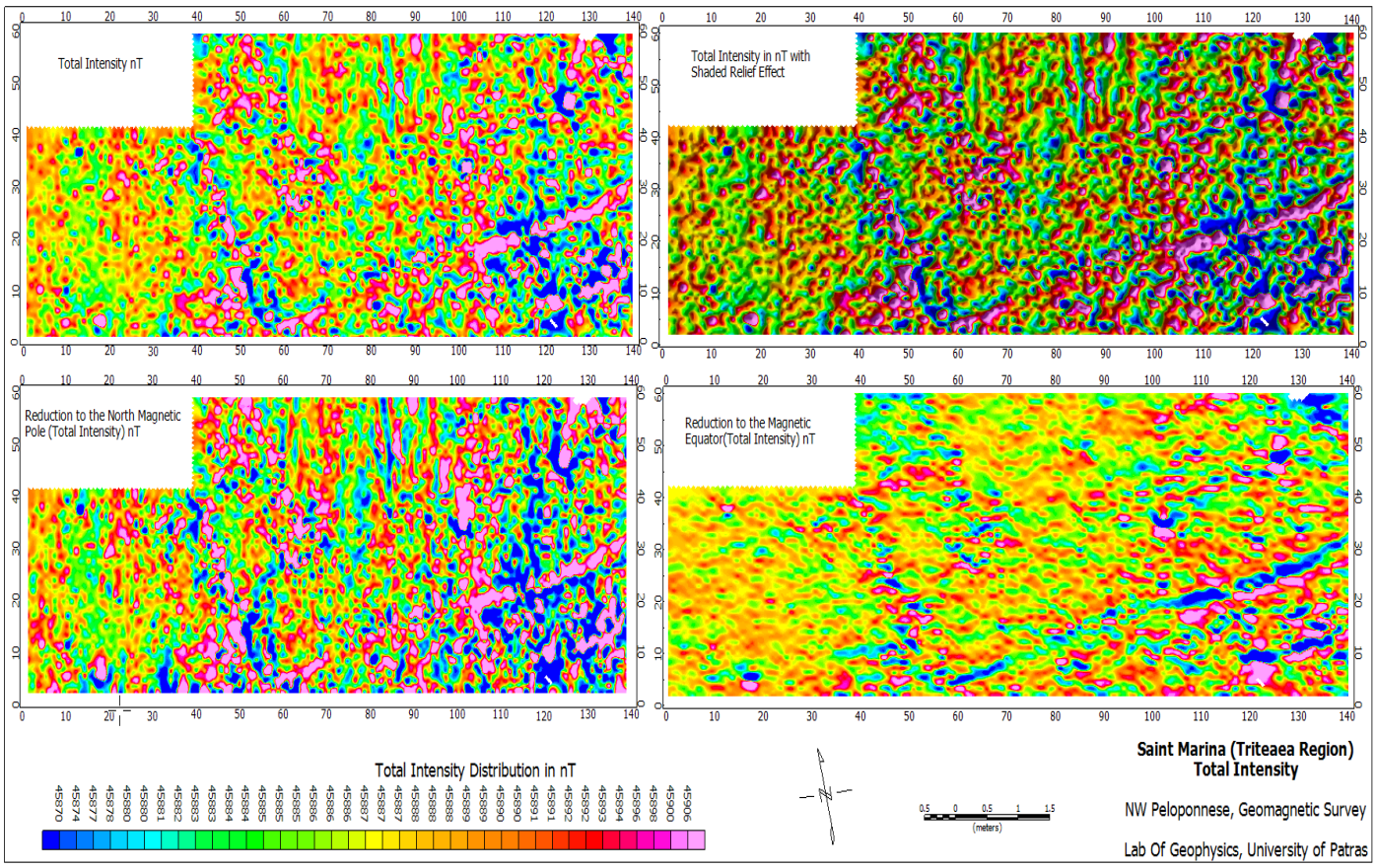

Figure 14. Presentation of total intensity with normal, shaded relief and reduction to the north magnetic pole and magnetic equator, where geomagnetic anomalies presented between 0.90 to 1.50 m depth.

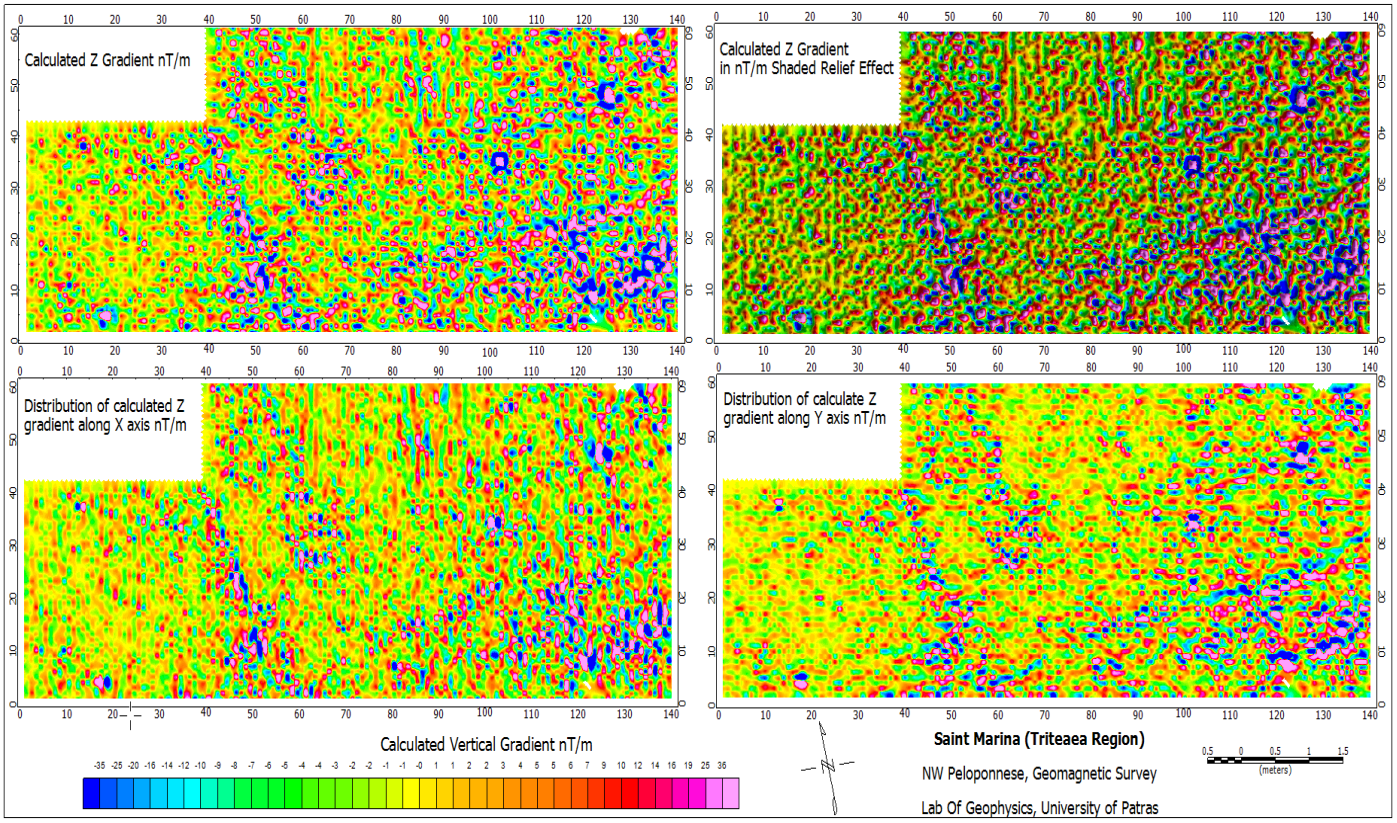

Figure 15. Presentation of calculated vertical gradient, application of shaded relief, geomagnetic anomalies along *X* and *Y* axes, between 0.90 to 1.5 m depth.

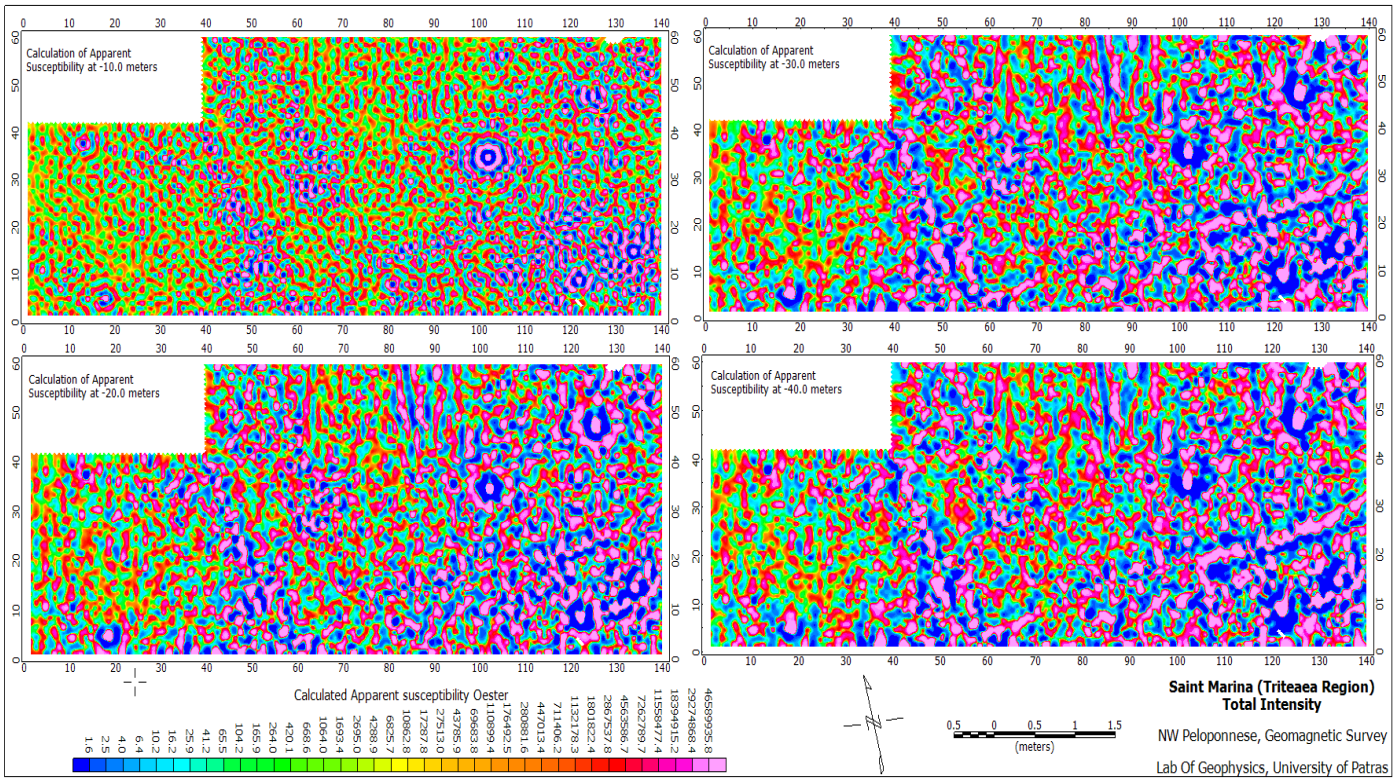

Figure 16. Calculation of apparent susceptibility from total intensity at −10, −20, −30, and −40 m depth.

By applying a specific mathematical filter on total intensity values, the apparent susceptibility distribution is calculated in **Figure 16**. Algorithms distributed that parameter between −10 and −40 m depth with a −10 interval. In low depths, apparent susceptibility seemed to be classified in two parallel parts, filled with many magnetic anomalies, which certified the existence of magnetized structures. In greater depths, apparent susceptibility was reported more emphasized with an increased number of magnetic bodies. Geometrical characteristics were notified with huge clarity; also, the existence of the cross-section of two parts was certified, which seemed like part of a corner. The variety of that property was between 1.6 and 46,589,934.8 oester.

Processing with the 3D mathematical algorithm illustrated in **Figure 17**. 3D Euler deconvolution after the correlation between magnetic elements and its gradients obtained the image of **Figure 15**. Measurements were processed gradually by rotation of the structural index between 0 and 3 with an interval equal to 1 (**Table 1**). According to the depth legend, geomagnetic sources were defined between 0.15 and 1.65 m. By utilizing a structural index with values of zero and one, there was growth of magnetized bodies with clear geometrical lines. Increasing structural index value at two and three, depth of magnetized bodies seemed to be stable at 1.65 m, with simultaneous reduction of magnetized structures. Also, geometrical characteristics were defined with a decreased ratio.

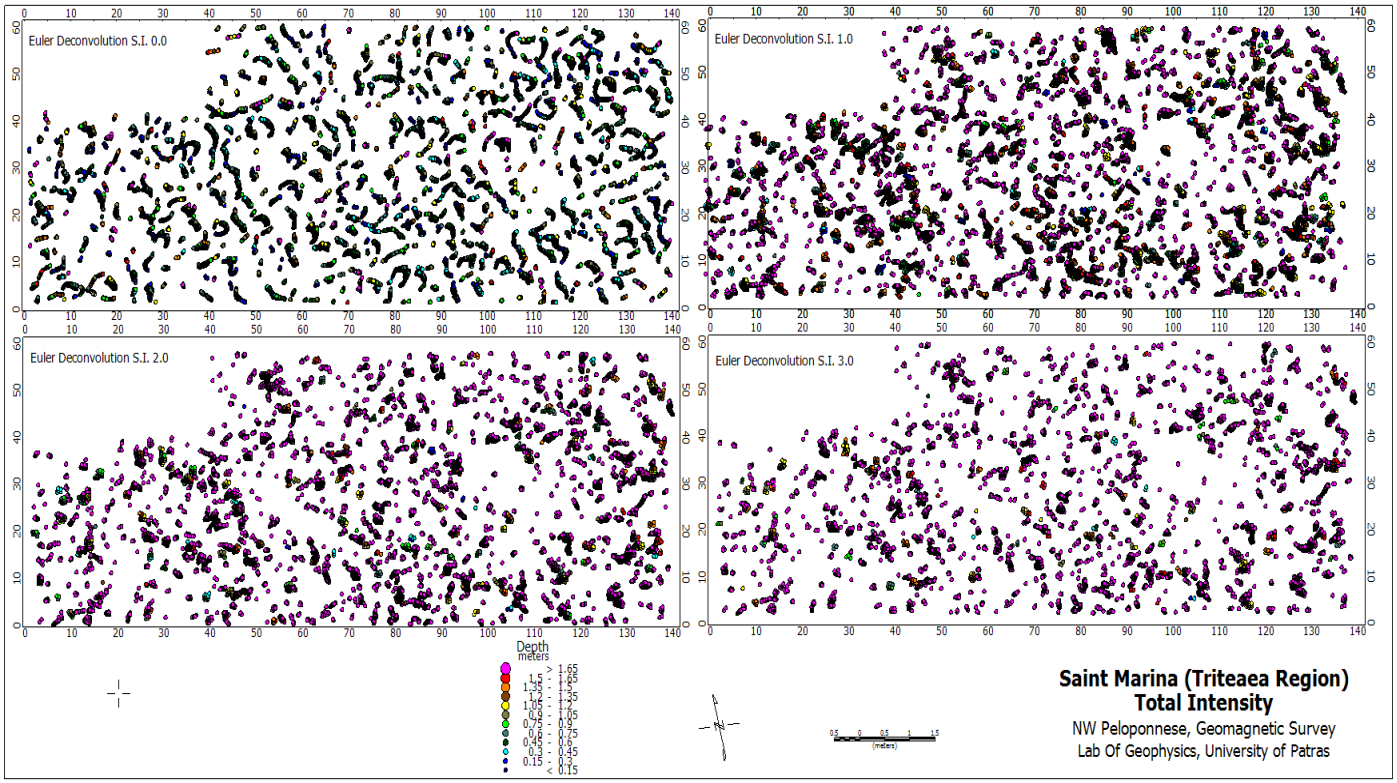

Figure 17. Application of 3D Euler deconvolution on total intensity measurements with S.I. at 0, 1, 2 and 3.

In **Figure 18**, the appearance distribution of the measured vertical gradient. That technique was applied on geophysical grids from the initial survey procedure. Vertical gradient refers to a very rapid technique that measures the vertical derivative of a magnetic field and contributes to the highlighting of horizontal magnetic structures.

After processing values with Oasis Montaj software, a huge number of magnetic structures were detected. Most of them were concentrated at the west part of the vertical gradient map. In conclusion, it seemed to be extracted from shaded relief processing and reduction to magnetic north and the equator. Unfortunately, there wasn't evidence of clear geometrical characteristics. By applying specific filters of Oasis Montaj software, the distribution of apparent susceptibility was calculated at −10, −20, −30, and −40 m depth (**Figure 19**). A huge concentration of increased magnetized structures occurred mostly at the west side of the vertical gradient map. Number of magnetized structures increasing analogously to depth value allocation.

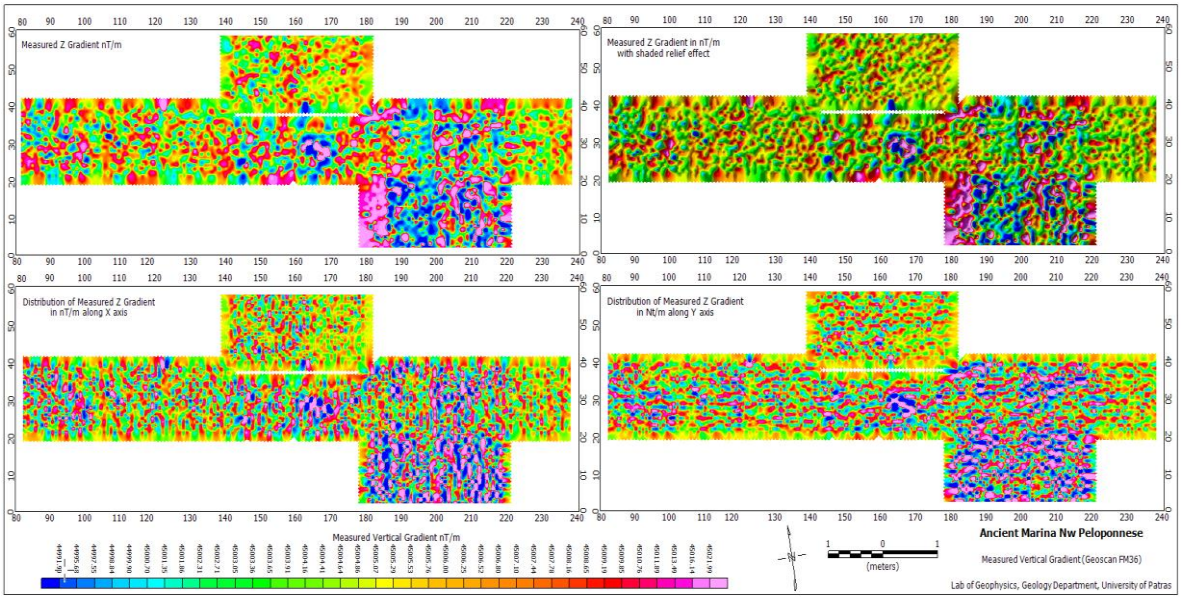

Figure 18. Presentation of measured vertical gradient, with shaded relief and reduction to the north magnetic pole and equator on the initial area, between 1.5 to 2.25 m depth.

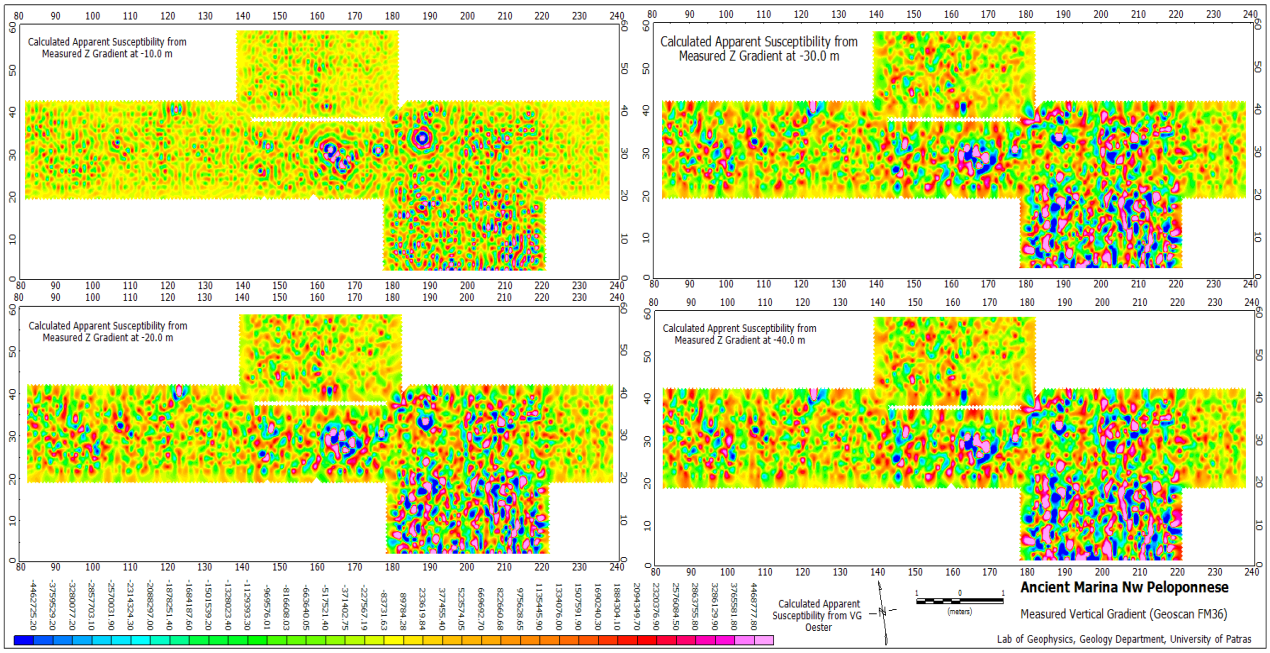

Figure 19. Calculation of apparent susceptibility on measured vertical gradient at −10, −20, −30, and −40 m depth on initial area between 1.5 to 2.25 m depth.

Further processing of vertical gradient values was implemented by utilizing the 3D Euler deconvolution mathematical algorithm (**Figure 20**). A mathematical approach was applied gradually by using four different structural indexes from 0 to 3 with an interval equal to 1 (**Table 1**). By processing values with an index equal to 1, the equation reported a few numbers of magnetized structures with geometrical characteristics. Most of them appeared by simultaneously increasing the structural index value. According to the depth legend, magnetized sources seemed to appear between 0.24 and 2.75 m in depth.

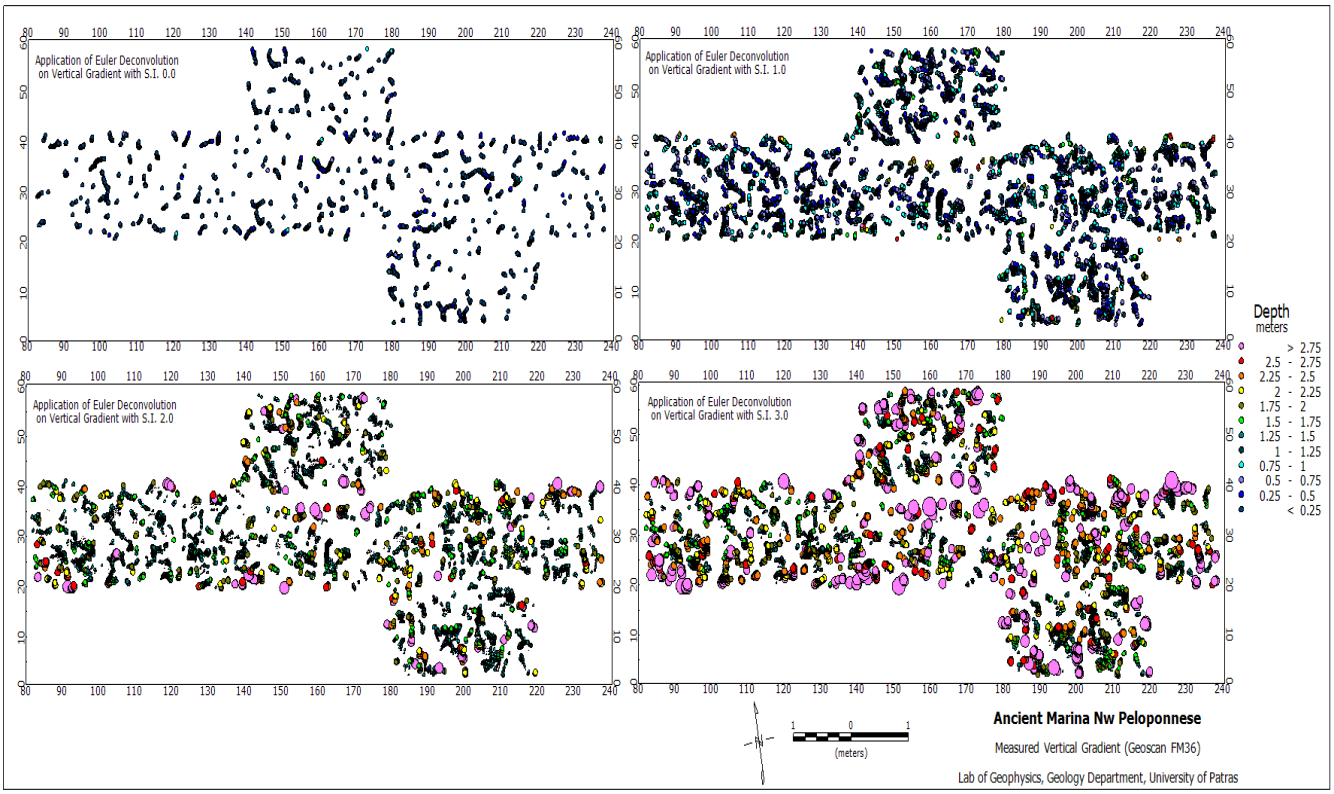

Figure 20. Application of Euler deconvolution on measured vertical gradient with S.I. at 0.0, 1.0, 2.0 and 3.0.

9. Discussion

In that section, results from interpretation will be discussed in detail. Measurements from field procedures were collected by adopting three different geophysical techniques. Each of them focuses on the distribution of specific physical properties. Geomagnetic prospecting was [41–43] obtained on separated geophysical grids, where data stations were located on parallel profiles along the south-north axis. Geophysical surveys on each grid began from the southwest corner. Profiles and discreet stations were investigated with one-meter intervals. For eliminating purposes of collected measurements, non-magnetic elements were used.

After the successful accomplishment of three techniques field procedures, grid data were combined through statistical analysis [9,32] based on the common average value according to the used technique.

9.1. Discussion on electric prospecting

Electric prospecting is utilized by performing a twin-probe arrangement, a technique independent from topographic allocations. The base station of the twin probe had been chosen in the intermediate line of geophysical grids away at fifteen times the mobile electrodes distance (**Figure 10**). In **Figure 13**, the result is depicted from soil resistance distribution in ohms. According to the color scale schedule, that property seemed to be valid between 18 and 67 ohms. Low soil resistance indicated by the existence of blue color (cold color). These formations presented high conductivity or, alternatively, underground targets in greater depth. In some cases, we detect cloudy geometrical characteristics. On the other hand, a huge extension of the map was covered by high values of soil resistance represented by red and purple colors (hot colors). Low conductivity indicated that the electric field met a bad current conductor. In most cases, there was an obvious existence of geometrical characteristics. Observers could easily recognize settlements consisting of corners (archaeological remains). By interpreting electric values with the shaded relief equation (**Figure 13**), geometrical characteristics were very well defined, a matter that divorced them from geological existence. By advanced interpretation of the same data field with the equation of the Fast Fourier Transform (**Figure 13**), more details were detected and some geometrical characteristics too. Application of shaded relief (**Figure 13**), certificated existence of geometrical characteristics, while noise was eliminated. The depth of the twin-probe array was limited to three times the internal pair distance. For example, in the case of an internal pair distance equal to 0.75 m, it means that the technique could detect the underground target until a 2.25 m depth.

9.2. Discussion of magnetic prospecting

Total intensity allocation is illustrated in **Figure 14**. According to the color scale, total intensity seemed to be valid between 45,870 and 45,900 nT. The intensity map was covered by a huge number of magnetic anomalies, which were extended all around the magnetic map. By careful observation, there were geometrical characteristics in the same position that were detected from electric prospecting. Certification of geometrical characteristics was done by the applied shaded relief procedure (**Figure 14**). In this map, magnetic anomalies were presented with greater clarity in relation to the initial total distribution. By calculating magnetic field parameters, total intensity measurements reduced to Magnetic North Pole (**Figure 14**) and Magnetic Equator (**Figure 14**). Both magnetic distributions illustrate the existence of magnetic anomalies and clear geometric characteristics.

Through a special mathematical filter calculation of the first derivative [37] from total intensity values, the result occurred in **Figure 15**. In that appropriation, geomagnetic anomalies seemed to be divided into smaller fragments. The existence of magnetic anomalies remains as it was in real distribution. Also, geometrical characteristics were well defined. By performing shaded relief procedures, corners of settlements were detected and certified, a matter that didn't present the existence of geological formations.

By further processing through a specific mathematical algorithm, a calculated allocation of apparent susceptibility [37] from total intensity values **Figure 16**.

Distribution of geophysical property observed in four different depths. Most of them are characterized by a great number of magnetized bodies that are lying across the cross-sections of two parts. Magnetic anomaly lengths seemed to be increasing relative to the depth value. Magnetic data were reduced to greater depth by performing downward continuation. Such a kind of interpretation is confluent at noise elimination, while attitude geomagnetic anomaly is towards its magnetic source.

Three-dimensional interpretation occurred by performing the Euler homogeneity equation on total intensity measurements (**Figure 17**). According to that equation, field magnetic parameters were combined with calculated gradients. The Euler equation is trying to reconstruct the magnetic source, which produced the current geomagnetic anomaly. The solution to that problem is effusive as a structural index. The solution from the Euler equation was depicted as a small circle. Tightened presentation of circles was accepted as a solution and indicated low deviation error. Also, the diameter of the circle corresponded to depth reporting. For simplicity purposes, color on the depth scale was selected with cold colors in low depths. Mean values represented a little warm color, while the highest depth values were indicated by warm colors. Euler deconvolution equation applied gradually by adopting four different structural index values. These were varied from 0 to 3 with intervals equal to one (**Table 1**). The existence of geometrical characteristics seemed to be valid at the first two values of the structural index. There were a huge number of geometrical remains that were recognized as circular anomalies. These findings were limited to 0.3 m in depth. By increasing the structural index value at 2 and 3, observed growths of geophysical anomalies from greater depths. These were represented by increased diameter circles, which were indicated by warm colors, with depth varying from 1.5 to 1.65 m.

The third technique (measured vertical gradient) was performed on an area from the initial survey. The vertical gradient consisted of a rapid technique that recorded the alteration of vertical components of the geomagnetic field. That technique is independent from daily geomagnetic drift but requires excellent adjustment of the fluxgate instrument on a quiet magnetic point [9,32]. Measurements were collected with the same procedure as in total intensity (profiles and stations distant at one-meter intervals along the South-North axis). That technique contributes to recording magnetized bodies in depth, which varies 3 to 5 times the sensor height (0.5 m) above the ground surface. In that case, the sensor was set at 0.5 m above ground, where penetration depth varied between 1.5 to 2.25 m. Differential magnetometer was an effort with the ability to distinguish in an excellent way the horizontal distribution of magnetized structures. Results from the interpreted procedure through Oasis Montaj software are depicted in **Figure 18**. The distribution of vertical gradient seemed to consist of many magnetic anomalies, concentrated at the west part of the map. Geometrical characteristics are absent from vertical gradient maps, except the center of the west area. That matter was certified from shaded relief implementation, where the indicated existence of clear geometrical remains in relation to the great number of magnetic anomalies (**Figure 18**). By adopting magnetic field parameters (inclination, declination), a calculated reduction to the north pole and magnetic equator. Reduction to the north magnetic pole **Figure 18** just confirmed the existence of magnetic bodies and pointed out that the number of geomagnetic anomalies seemed to be increased in

the west part of the vertical gradient map. Unfortunately, the existence of geometrical characteristics wasn't certified by that mathematical filter. Reduction to the magnetic equator **Figure 18** didn't appear any more details related to geometrical remains, which were absent. Instead of this, confirmed the existence of magnetized structures by presentation of a huge number of geophysical anomalies. Most of them were concentrated on the west area of the vertical gradient map. Measured vertical gradient varied between 4,499,199 and 4,502,199 nT/m.

The existence of magnetized bodies in that area is confirmed by the calculation of apparent susceptibility from vertical gradient values (**Figure 19**). Distribution of apparent susceptibility was examined in four different depths. These were varying between −10 and −39 with an interval equal to −10. For comparison purposes, developed a common color scale zone and scale. According to the color scale bar, apparent susceptibility seemed to be varied—−4,462,624.20 to 4,468,777.80 oester. At depths of −10 m, apparent susceptibility is represented by a few points that were observed increasing in values and characterized as circular anomalies. Increasing property values were detected at −20 m depth. Most of the highest values were concentrated in the west part of the area with an extension at the south. At −30 and −40 m depth, the distribution of apparent susceptibility seemed to reach the highest values with simultaneous growth of circular anomalies. In four depths, there is the appearance of many magnetic dipoles. Geometrical characteristics were absolutely absent.

Depth of existing structures indicated by implementing the 3D Euler Deconvolution algorithm (**Figure 20**). Processing of measured vertical gradient values occurred by adopting four different values of structural index. That parameter applied by using values that varied from zero to three with one interval. The solution of Euler deconvolution with a structural index equal to zero had as a result the appearance of a few magnetized bodies with geometrical characteristics in specific locations. Structures seemed to be located between 0.24 and 0.5 m in depth. By adopting a higher structural index like one, the number of magnetized bodies increased. Observed growth of geometrical remains; the existence of corners and circular anomalies was certified. These findings were located until 1.5 m depth. By adopting structural index 2 and 3, a decreasing number of magnetized bodies were observed. The depth of magnetized bodies was equal to 2.75 m with certified existence of geometrical characteristics.

10. Conclusion

Combined geophysical investigation performed on the territory of NW Peloponnese. Specific detailed electric and magnetic prospecting was utilized in the Saint Marina area, where it was believed that there were buried settlements of Ancient Tritaea.

Geophysical surveys focus on discreet geophysical grids that were established on the ground surface by non-magnetic materials. Two main geophysical approaches were combined for the detection of underground archaeological remains. Both electric and magnetic techniques are applied with non-destructive allocation.

For simplicity purposes, data from both geophysical techniques were combined in a mosaic distribution. Grid connection applied by reduction of values on common average through statistical analysis.

Through specific software such as Oasis Montaj, data interpretation is accomplished gradually. Measurements were dimensioned with specific coordinates (level/geographical) according to grid position and area extension. Distribution of measured physical property occurred on a color scale format. That main processing is applied to electric and magnetic measurements. The highest details were observed by the applied shaded relief procedure.

Further processing was performed on magnetic measurements. The main scope was the definition of non-geological formations. Reduction to the north pole, equator, and calculation of apparent susceptibility obtained through specific algorithms after computation of magnetic field properties. By interpreting measurements with the above mathematical filter, a certified existence of magnetized bodies. Also, clear geometric characteristics are defined on the above maps, a matter that divorces them from the existence of geological structures. Three-dimensional filter through Euler deconvolution equation applied on magnetic measurements through advanced processing. By that mathematical equation, observed growth of clear geometric characteristics corresponded to remains of archaeological settlements. By using such a kind of mathematical filter, the cause that produced the magnetic anomaly was detected, while estimating the depth of the magnetic source, which was between 1.5 and 2.7 m. Best results were obtained by applying a structural index equal to 0 (magnetic contact).

Electric mapping and magnetic prospecting combine excellently in that geophysical problem. Electric fields divided the area into low and high-interest subareas and detected possible underground targets. The existence of them was confirmed by magnetic prospecting, which was applied by proton and differential magnetometers. Confirmation of findings through more than one geophysical technique constitutes a required target.

Magnetic techniques certify the results from electric mapping. Both total intensity and vertical gradient distribution presented the existence of geometrical characteristics in that area. Also, the three independent techniques illustrated the continuation of existing archaeological remains since 1988 with the current geophysical survey.

Electric mapping, total intensity, and vertical gradient are techniques characterized by non-destructive implementation with excellent results. Researchers should bear in mind that magnetic prospecting must be applied by using no magnetic elements. Also, except for unmagnetized materials and elements, researchers must be unmagnetized.

Geophysical research is still active in this area. The geophysical team is waiting for a new request for a geophysical survey from the Archaeological Service of Achaea. Geophysical research can be applied to any problem on the ground surface in a non-destructive way. Results from geophysical investigation can drive the archaeological hoe exactly on the subsurface target by saving money and accidental excavation.

Author contributions: Conceptualization, PS and SP; methodology, PS; software, PS; validation, PS, JB and CK; formal analysis, PS; investigation, PS, CK and JB; resources, PS; data curation, PS; writing—original draft preparation, PS; writing—review and editing, PS; visualization, PS; supervision, PS and SP; project administration, SP and PS; funding acquisition, SP and LM. All authors have read and agreed to the published version of the manuscript.

Institutional review board statement: Not applicable.

Informed consent statement: Informed consent was obtained from all subjects involved in the study.

Conflict of interest: The authors declare no conflict of interest.

References

1. Barbolla DF, Miccoli I, Ditaranto I, et al. Geophysical Surveys to Highlight Buried Ancient Walls of Ugento (Lecce, Italy). NDT. 2024; 2(3): 204–213.
2. Kainz J. An Integrated Archaeological Prospection and Excavation Approach at a Middle Neolithic Circular Ditch Enclosure in Austria. In: Digital Methods and Remote Sensing in Archaeology, Archaeology in the Age of Sensing. Springer; 2016.
3. Křivánek R, Čižmář I. Verification of Geophysical Surveys by New Archaeological Excavations on the Grounds of the Middle La Tène Site of Němčice in 2021–2022. Natural Sciences in Archaeology. 2024; XV(1): 30–39. doi: 10.24916/iansa.2024.1.2
4. Křivánek R, Tirpák J. Geophysical Survey and Changes in the Use of the Cultural Landscape. Interdisciplinaria Archaeologica Natural Sciences in Archaeology. 2023; XIV(1): 9–28. doi: 10.24916/iansa.2023.1.1
5. Peter M, Tencer T, Vágner M, et al. Geophysical Survey of the Hillfort Staré Zámky near Brno-Líšeň, Czech Republic. Natural Sciences in Archaeology. 2020; XI(2): 183–195.
6. Papamarinopoulos S, Papaioannou MG, Stefanopoulos P, Bafitis X. The Geophysical Discovery of a Second World War Battlefield in Central Crete During Construction Activities by a Building Company. The Solution to a Major Environmental Problem. In: Proceedings of the Symposium on the Application of Geophysics to Engineering and Environmental Problems; 23–26 April 1995; Orlando, FL, USA
7. Papamarinopoulos St.P., Tsokas G.N., Lakaki M., and Savopoulou T. Advanced Geophysical Processing of Field Data and Practical Results. Geophysical Exploration of Archaeological Sites-Series. In: Theory and Practice of Applied Geophysics. Vieweg Publishing; 1993. pp. 149–157.
8. Papamarinopoulos S, Stefanopoulos P, Papaioannou M. Geopysical investigations in search of ancient Helike and the protection of the archaeological site versus the rapid building expansion. In: International Symposium on Engineering Geology and Underground Construction. Springer; 1997
9. Stephanopoulos P, Papamarinopoulos S. Geoelectric, geomagnetic and vertical gradient investigation on Knossos area, Crete Island for detection of archaeological settlements. Journal of Geography and Cartography. 2024; 8(1): 10310. doi: 10.24284/jgc10310
10. Trinks L, Larsson M, Gabler E, et al. Thorén. Large-Scale Archaeological Prospection of The Iron Age Settlement Site Uppåkra-Sweden. In: Archaeological Prospection Proceedings of the 10th International Conference on Archaeological Prospection Vienna. Austrian Academy of Sciences Press; 2013
11. Milo P, Vágner M, Tencer T, Murín I. Application of Geophysical Methods in Archaeological Survey of Early Medieval Fortifications. Remote Sensing. 2022; 14(10): 2471. doi: 10.3290/rs14002471
12. Abudeif AM, Abdel Aal GZ, Ramadan HS, Al-Arifi N, et al. Mohammed. Geophysical Prospecting of the Coptic Monastery of Apa Moses Using GPR and Magnetic Techniques: A Case Study, Abydos, Sohag, Egypt. Sustainability. 2023; 15(14): 11119
13. Gibson T. Magnetic prospection on prehistoric sites in Western Canada. Geophysics. 1986; 51(3): 553 – 560.
14. Olorunfemi MO, Ogunfolakan BA, Oni A. Geophysical and Archaeological Survey in Igbo Oritaa (Iwo), Southwest Nigeria. African Archaeological Review. 2019; 36(1). doi: 1007/s10437-019-09357-7

15. Yulianto T, Irham MN, Sasongko DP, Widada S. 3D modeling of subsurface jiwo fault around gantiwarno subdistrict, klaten district, central java using the magnetic method. Journal of Physics: Conference Series. 2020; 1524(1): 012035.
16. Bescoby DJ, Cawley GC, Chroston PN. Interpretation of Geophysical Surveys of Archaeological Sites using Artificial Neural Networks. Conference Paper. IEEE Xplore. 2003; doi: 10.1109/IJCNN.2003.1223850
17. Fassbinder JWE, Hahn S, Parsi M. Geophysical Prospecting on Soils in Mesopotamia: From Mega-Cities in the Marches of Southern Iraq to Assyrian Sites in the Mountains of Kurdistan. In: World Archaeo-Geophysics. Springer Nature; 2024.
18. Mekkawi M, Arafa-Hamed T, Abdellatif TF. Detailed magnetic survey at Dahshour archeological sites Southwest Cairo, Egypt. NRIAG Journal of Astronomy and Geophysics. 2013; 2(1): 175–183. doi: 10.1016/j.nrjag.2013.06.020
19. Ahmed SB, El Qassas RAY, Abed El Salam HF. Mapping the possible buried archaeological targets using magnetic and ground penetrating radar data, Fayoum, Egypt, The Egyptian Journal of Remote Sensing and Space Science. 2020; 23(3): 321–332.
20. Grassi S, Morreale G, Lanteri R, et al. Integration of Geophysical Survey Data for the Identification of New Archaeological Remains in the Subsoil of the Akrai Greek Site (Sicily, Italy). Heritage. 2023; 6(2): 979–992.
21. Wilhelm A. Honorary resolution found in the Epigraphic Museum (German). In: New contributions to Greek epigraphy. Forgotten Books; 2018.
22. Rizakis A. The Achaean Cities: Epigraphy and History (French). Center for Research on Greek and Roman Antiquity, National Foundation for Scientific Research; 2008.
23. Wilhelm A. New contributions to Greek epigraphy (German). Forgotten Books; 2018
24. Nerandzoulis P. Achaean Dodecapolis ruins and monuments I Tritaia. Internal Publication Archaeological Service; 1938. pp. 19–22.
25. Lakaki M. A.D.42, Chronicles B1. Archaeological Service; 1992. p. 161.
26. Institute of Geology and Mineral Exploration. Goumeron Sheet Geological Map. Institute of Geology and Mineral Exploration; 1981.
27. Butler D, Liopis J, Briuer F. Geophysical and Archaeological Investigations for Location of a Historic Cemetery, Fort Stewart, Georgia. US Army Corps of Engineers Waterways Experiment Station Miscellaneous Paper; 1993.
28. Saleh S, Saleh A, El Emam AE, et al. Detection of Archaeological Ruins Using Integrated Geophysical Surveys at the Pyramid of Senusret II, Lahun, Fayoum, Egypt. Pure and Applied Geophysics. 2022; 179(5): 1981–1993. doi: 10.1007/s00024-022-02910-2
29. Branko M, Jana H, Dimc F. Comparison of different geophysical techniques in relation to archaeological data for settlement reconstruction - the case study of Nauportus. Slovenia; 2007.
30. Bevan B. A Geophysical Survey at the West House, Richmond National Battlefield. Technical Report; 2002.
31. Bayowa OG, Fawole O, Olorunfemi MO, et al. Magnetic and resistivity imaging of a probable fault within the Precambrian crystalline rocks in Ogbomoso, Southwestern Nigeria. Contributions to Geophysics and Geodesy. 2024; 54(2): 167–189. doi: 10.30577/congeo.2024.54.2.3
32. Stephanopoulos P. Contribution of geophysics in solution of archaeological and environmental problems [PhD Thesis]. University of Patras; 2002.
33. Almajid Maan Hasan Abdullah, Marwan Mutib. A New Comprehension of the Basement Undulation in North Iraq Resorting to Geomagnetic Investigation, Geological Bulletin of Turkey,62 (2019) 199-216
34. Gaweish W, Marzouk H, Petrov AV, et al. Magnetic data interpretation to determine the depth of basement rocks and structural elements of Mandisha village, El-Bahariya Oasis, Western Desert, Egypt. News of the Ural State Mining University. 2019; 2(54): 7–19. doi: 10.21439/2297-2091-2019-2-7-19
35. Abubakar S, Muhammad SB. Upward continuation of total magnetic field intensity data over Sokoto basin, north-western Nigeria. Caliphate Journal of Science & Technology. 2023; 5(2):148–153. doi: 10.4304/cajost.v5i2.9
36. Bonsall J. New Global Perspectives on Archaeological Prospection. Archaeopress Publishing; 2019.
37. Manual Oasis Montaj 2008, Mapping and Processing System. Available online: https://www.geosoft.com (accessed on 12 January 2025).
38. Augie AI, Salako KA, Rafiu AA, Jimoh MO. Geophysical Magnetic Data Analyses of the Geological Structures with Mineralization Potentials Over the Southern Part of Kebbi, NW Nigeria. Mining Science. 2023; 29(2022): 179–203. doi: 10.36190/msc222811

39. Lichtenberger A, Meyer C, Schreiber, Zardaryan MH. Magnetic Prospection in the Eastern Lower City of Artashat-Artaxata in the Ararat Plain of Armenia. Electrum. 2022; 29: 109–125. doi:10.4467/20800909EL.22.008.15778
40. Hahn SE, Fassbinder JWE, Parsi M, et al. Magnetic prospection close to the magnetic equator: Case studies in the Tigray plateau of Aksum and Y eha, Ethiopia. In: Proceedings of the 13th International Conference on Archaeological Prospection; 27 August–1 September 2019; Sligo, Ireland.
41. Mušič B, Horvat J, Dimc F. Comparison of different geophysical techniques in relation to archaeological data for settlement reconstruction—the case study of Nauportus. In: Proceedings of the Archaeology and Computers, Workshop 12: Cultural Heritage and New Technologies; 5–7 November 2007; Wien, Slovenia.
42. Türkiye J, Bülteni, Araştırmayla J, et al. A New Comprehension of the Basement Undulation in North Iraq Resorting to Geomagnetic Investigation. Geological Bulletin of Turkey. 2019; 62(199): 216.
43. Hannian S, Hijab B, Laftah A. Geophysical Investigation of Babylon archeological City, Iraq. Diyala Journal for Pure Science. 2021; 17(3): 1–24. doi: 10.24236/djps.17.03.532c